# Coil Springs with Constrained Layer Visco-elastic Damping for Passive Isolation.

Eric R. Ponslet[a] and William O. Miller[b]

Hytec, Inc.
110 Eastgate Drive, Los Alamos, NM 87544

## ABSTRACT

This paper summarizes the design, optimization, development, fabrication, and testing of a vacuum compatible coil spring with embedded constrained layer visco-elastic damping. The spring is developed as part of the NSF funded LIGO (Laser Interferometer Gravity Wave Observatory) project. Large numbers of those springs are the primary components of multi-stage, in-vacuum, passive seismic isolation stacks that provide high attenuation (-160 dB/decade above 15 Hz) of floor vibrations for ultra-sensitive (better than $10^{-18}$ m/$\sqrt{\text{Hz}}$ noise floor between 40 and 1000 Hz) laser interferometers.

The spring design addresses both requirements for passive isolation within a single, self-contained, vacuum tight envelope: low stiffness for maximum attenuation and non-viscous damping to limit resonant amplitudes in the stack. This is achieved with a tubular coil spring design with an internal torsional constrained layer damping structure.

The paper presents the analysis of this spring using closed-form analytical expressions, trend studies showing the strong dependence of spring performance on key design parameters, and explicit numerical design optimization. Manufacturing issues are briefly discussed. Finally, experimental results from static and dynamic tests performed on prototype units are presented. Results show loss factors of the order of 1.5% in the transverse direction to 3% in the axial direction, at frequencies from 1 to 2 Hz.

**Keywords:** Coil Spring, Damping, Vibration Isolation, Constrained Layer, Design Optimization

## 1. INTRODUCTION

Vibration isolation systems are widely used to reduce transmission of floor vibrations to sensitive optical experiments. In passive systems, isolation is achieved by inserting soft mechanical links (isolators) between the source of the vibration (usually the laboratory floor) and an optics table that serves as a base for the experiment. The effectiveness of an isolation system is measured in terms of transmissibility functions $T$ which give a measure of the relative amplitudes of optics table vibration to floor vibration. For a properly designed isolation system, the magnitude of the transmissibility functions resembles the curve shown in Fig. 1.

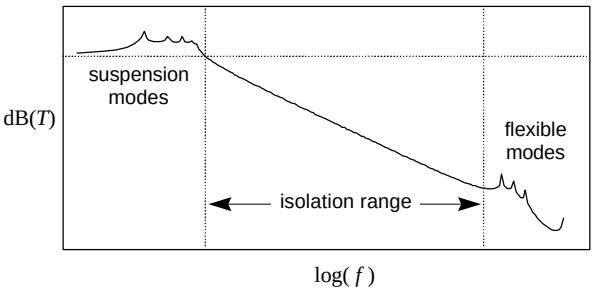


**Figure 1: Typical transmission characteristics of an isolation system.**

Three regions can be distinguished in the figure. At "low" frequencies, resonant peaks corresponding to the suspension modes are observed. There is no isolation in this band (in fact there is amplification). At the "high" end of the spectrum, flexible modes of the supported and/or supporting structure themselves produce other resonant peaks. In a properly designed isolation system, those two frequency ranges are separated by a wide "isolation band" where transmission decays rapidly with frequency $f$ (about -40dB/decade for a lightly damped, single stage system). In the isolation band, the

[a] Director of Research; E-mail: ponslet@hytecinc.com; Telephone: (505) 662-7329; Fax: (505) 662-5179.
[b] President; E-mail: womiller@hytecinc.com.

transmissibility is a direct function of the "softness" of the isolator mounts. This "softness" can be expressed by a *characteristic deflection* parameter $d_{max}$. For usual applications, were the isolators also support the weight of the device, $d_{max}$ is defined as

$$d_{max}(f) = \frac{P_{max}}{|k(f)|}, \tag{1}$$

where $P_{max}$ is the maximum static load that can be supported by the isolator and $k$ is the stiffness of the isolator. Note that $k$ may be a frequency-dependent quantity (as is the case with rubber isolators for example).

At lower frequencies however, resonances of the suspension dominate the transmissibility. To properly dampen the response to transients, isolation systems must also provide some damping. That damping is usually expressed in terms of the *quality factor* ($Q$) of a resonant mode. The $Q$ defines the dynamic amplification at resonance (ratio of dynamic to static response) and is equal to

$$Q(f) = \frac{1}{h} = \frac{1}{2z}, \tag{2}$$

where $h$ is the loss factor and $\zeta$ the critical damping ratio of the mode considered. The $Q$'s of the suspension are directly controlled by the loss factors of the isolators. Examples of high loss isolators include rubber supports or spring/damper combinations. Note also that viscous damping (dashpots in vehicle suspensions for example) is less than ideal in isolation applications because of the stiffening effect at high frequencies, which leads to loss of isolation performance. Visco-elastic damping is in general preferable because of lesser stiffening.

In short, soft mounts for high performance isolation systems must have the following characteristics: large characteristic deflections in the isolation range (typically above 1 to 15 Hz), and high loss in the resonance region (typically below 1 to 15 Hz). Other desirable characteristics are compactness and simplicity, low drift, good aging characteristics in a variety of environments, and low outgassing potential in the case of high vacuum applications.

The LIGO project[1] (Laser Interferometer Gravity wave Observatory) is currently building very large (4 km arm length) Fabry-Perot interferometers designed to detect and measure gravity waves. Gravity waves passing through the instrument are expected to produce the equivalent of about $10^{-18}$ meter perturbations in the 4 km distance between hanging mirrors. To achieve adequate sensitivity, extreme care must be taken to reduce all sources of noise in the instrument. One such source is of course the random seismic vibrations present in the floor of the detector facility.

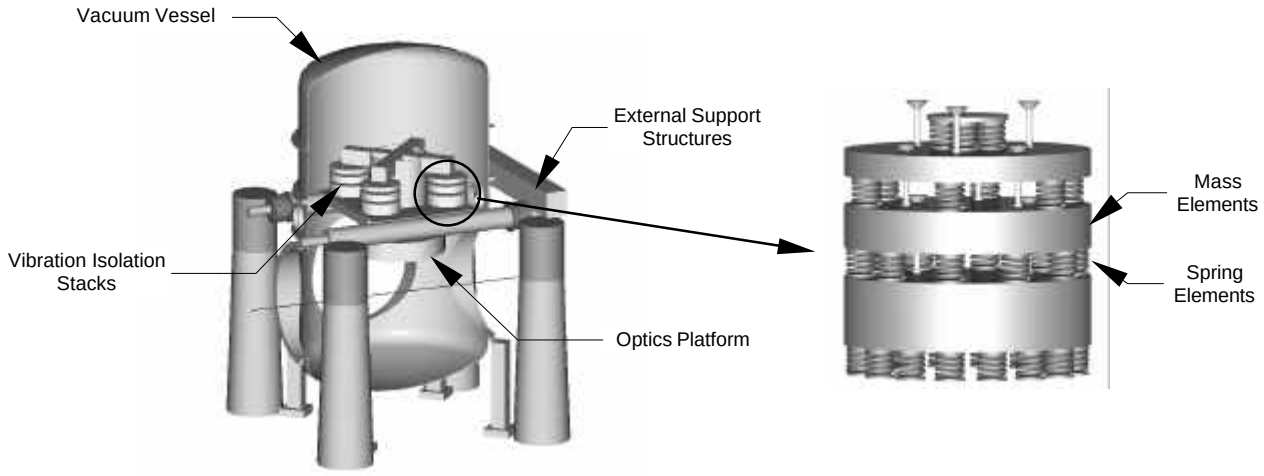


**Figure 2: LIGO vacuum vessel with external support structure and seismic isolation stacks (left hand cross beam removed and only one half of vacuum vessel shown).**

LIGO will number around 30 ultra-quiet optical platforms mounted inside vacuum chambers throughout the detectors. A typical design layout for these chambers is shown in Fig. 2. The seismic isolation elements are sitting entirely inside the vacuum envelope to avoid acoustic "shorting". They consist of multi-stage, passive isolation stacks of soft isolators and heavy masses. One of many technological challenges in the detector design relates to those isolators. They must achieve very low stiffness and relatively high damping while satisfying very strict outgassing limits. Early prototypes made use of cylindrical blocs of Fluorel[2] rubber (a low outgassing fluoro-elastomer). These isolators had very low $Q$ but

were fairly stiff, with a strong stiffening effect with increasing frequencies. Stacks designed around those springs did not meet the LIGO seismic isolation requirements.

The damped coil spring described in the next section provides a much softer alternative. The spring design addresses both requirements for passive isolation within a single, self-contained, vacuum tight envelope: low stiffness for maximum attenuation and non-viscous damping to limit resonant amplitudes in the stack. This is achieved with a tubular coil spring design with an internal torsional constrained layer damping structure. The spring "wire" is made (from the outside in) of a load bearing outer tube, a layer of visco-elastic material, and a sectioned inner tube as a constraining layer. The ends of the outside tube are sealed with a metal cap welded to the outer tube to provide a vacuum compatible spring. Stacks designed with this new spring meet the LIGO transmissibility requirements and the requirements on the $Q$ of the suspension modes (i.e. $Q < 70$ or so).

## 2. DAMPED COIL SPRING

Several spring concepts were considered in early stages of development. Compared to other types of springs, compression coils can provide relatively large deflections and load capacities, are relatively easy to manufacture, and do not fail catastrophically: in case of yield they simply compress all the way to solid length (the length of the spring compressed so that each coil is in contact with the next). Their simple outside geometry also lends itself to thorough chemical cleaning as required for ultra-high vacuum applications. Simple concepts for integrating damping treatments inside coil springs have been proposed in the past. Some involve friction between elements inside the coil[3] or energy dissipation through plastic deformations of internal fillers (lead for example). Although this can provide significant damping of deformations of large amplitude, the damping vanishes at the arbitrarily small amplitudes found in high performance isolation systems.

A variation on these concepts consists of filling a metallic tubular coil spring with a high damping visco-elastic material. However, simple calculations show that as long as the metal tube carries the largest part of the static load (which is desirable to avoid excessive creep), such designs are unable to produce the required amount of damping. A possible improvement consists of adding longitudinal fibers in the core[4]. Another approach consists of amplifying the mechanical coupling between the load bearing structure (the tube) and the visco-elastic material through *constrained layer damping* (CLD)[5]. CLD consists of inserting a very thin layer of visco-elastic material between the load bearing structure and a stiff constraining layer. Small relative motion between the load bearing and constraining surfaces induce large shear strain through the thickness of the thin visco-elastic layer.

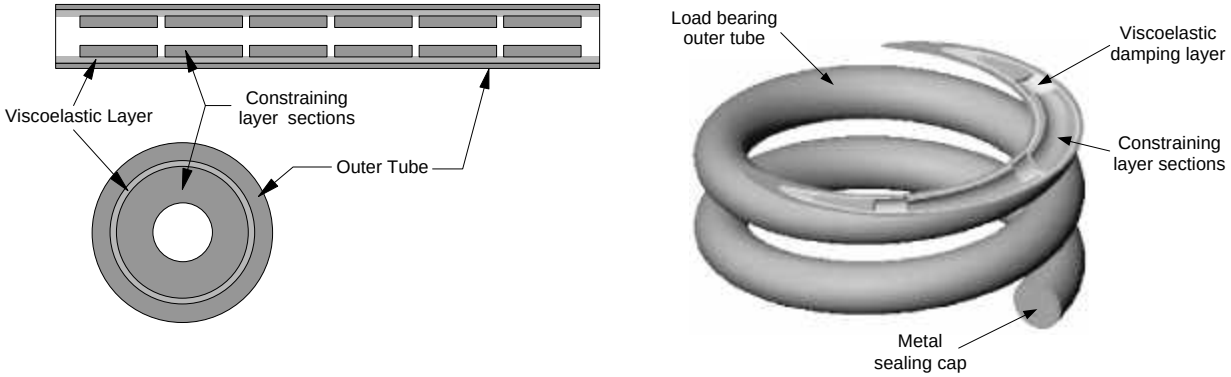


**Figure 3: Multi-layer tubular CLD coil spring concept[†]. The right hand view shows the bottom of a coil spring, cut by a plane orthogonal to the coil axis.**

Constrained layer damping (CLD) is traditionally used to damp plate and shell type structures[5]: a thin visco-elastic sheet with a thin metal backing sheet is glued directly on the structure. This concept must be adapted for use in the proposed tubular coil spring, in particular to avoid any exposure of the visco-elastic layer to the vacuum environment. A natural (but complicated) solution is to apply the damping treatment and constraining layer on the *inside* of the load carrying tube. The ends of the tube can then be sealed to completely enclose the damping material. The simplest configuration would consist of a continuous inner tube (the constraining layer) wrapped in a thin layer of visco-elastic material and trapped inside the outer load bearing tube. Since a coil spring is essentially a torsion bar, a twisting moment applied to the ***outer*** tube induces a twist angle differential between the inside and outside tube, shearing the visco-elastic layer. If the visco-elastic layer is thin, the shear strains are large and significant amounts of elastic energy are dissipated into heat.

[†] U.S. Patent pending, #08972030, filed Nov. 17, 1997.

Although this concept is adequate for a ***straight*** torsion bar, it cannot provide damping in a coil spring because of geometric coupling between the outside and inside tubes. When a coil spring is compressed, the pitch of the helix is reduced. This reduction in pitch geometrically dictates the twist angles of every section along the spring "wire". In a 3 layer CLD spring, since the inner tube is captive inside the outer tube, the twist angles are the same in both, and shear through the thickness of the visco-elastic layer does not appear.

Shear stresses in the visco-elastic layer can be recovered if geometric coupling is eliminated (or largely reduced) by using a series of "short" (much shorter than a full turn of the coil) sections of constraining tube instead of a continuous one, as shown in Fig. 3.

Note also that, just like in a classical flat plate CLD design problem[6], there is an optimal length for the constraining layer that maximizes damping, even for a straight CLD torsion bar. The reason for the existence of this optimal length is one of balance between the shear stiffness of the visco-elastic layer and the torsional stiffness (extensional stiffness in a flat plate problem) of the constraining layer. This will be examined in more detail further (section 5.1). The point is that even in a straight torsion rod without geometric coupling, there are performance justifications for using a discontinuous constraining layer instead of a continuous one.

## 3. TORSIONAL CONSTRAINED LAYER DAMPING ANALYSIS

### 3.1 Analysis

The state of stress in the cross section of the "wire" of a compression coil spring with a spring index $c$ (ratio of mean diameter of the coil to outside diameter of the spring wire) larger than about 5, and subject to an axial compression force $P$ is almost identical to that of a straight torsion bar subjected to a twisting moment $T = PD/2$, where $D$ is the mean coil diameter of the spring[7]. With this in mind, we analyze the 3 layer CLD spring by considering the balance of twisting moments along the length of a single inner constraining section (Fig. 4). The cross section is defined by the inner and outer diameters of the outside tube, $d_w$ and $D_w$, the inner and outer diameters of the constraining tube sections, $d_c$ and $D_c$, the shear moduli of the inside and outside tubes, $G_c$ and $G_w$, and the shear storage modulus and loss factor of the visco-elastic layer, $G_v'$ and $h_v$[‡].

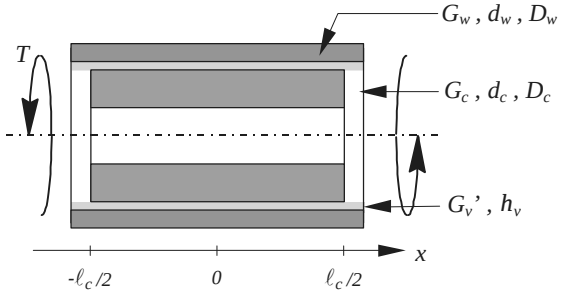


**Figure 4: Analysis of the tubular multi-layer CLD torsion rod.**

In addition, the following assumptions are made:

- no geometrical coupling between outside and inside tube. This is true for a straight torsion rod and a reasonable assumption for a coil as long as the length $\ell_c$ of the inner tube sections is much smaller than a full turn of the coil, i.e. $\ell_c << pD$ (where $D$ is the mean coil diameter).
- the thickness $t_v$ of the visco-elastic layer is small relative to its mean diameter, i.e. $d_v = (D_c + d_w)/2 >> t_v$.
- the axial extent of the gap between inner tube sections is neglected.
- the visco-elastic material is assumed much softer than the inside and outside tube materials, i.e. $G_v', G_v'' << G_w, G_c$, so that the direct torsional stiffness of the visco-elastic layer can be neglected.

Writing approximate torsional equilibrium of a "slice" of a segment of length $dx$, we have

$$T_w + T_c = T\ , \tag{3}$$

$$\frac{dT_c}{dx} = G_v'(1 + ih_v)\frac{pd_v^3}{4t_v}(q_c - q_w)\ , \tag{4}$$

[‡] The elastic modulus of a visco-elastic material is usually expressed as a complex number $G(f) = G'(f) + G''(f) = G'(f)\,(1 + i\,h(f))$ where $G$, $G'$, $G''$, and $h$ are frequency dependent quantities. $G'(f)$ is the storage modulus, $G''(f)$ the loss modulus, and $h(f)$ the loss factor.

where $T_c$ and $T_w$ are the twisting moments at $x$ in the inner and outer tube cross sections, respectively, $q_c$ and $q_w$ are the corresponding twist angles, $t_v = (d_w - D_c)/2$ and $d_v = (d_w + D_c)/2$ are the thickness and mean diameter of the visco-elastic layer, and $i = \sqrt{-1}$.

Using $T_c = G_c J_c \dfrac{dq_c}{dx}$ and $T_w = G_w J_w \dfrac{dq_w}{dx}$, where $J_c$ and $J_w$ are the torsional moments of inertia of the inner and outer tubes, respectively, and differentiating (4) gives,

$$\frac{d^2 T_c}{dx^2} - G_v'(1+ih_v)\frac{pd_v^3}{4t_v}\frac{G_w J_w + G_c J_c}{G_w J_w G_c J_c} T_c = -G_v'(1+ih_v)\frac{pd_v^3}{4t_v}\frac{T}{G_w J_w}, \tag{5}$$

which is integrated with respect to $x$ to give

$$T_c = T\frac{G_c J_c}{G_w J_w + G_c J_c}\left(1 - \frac{\cosh(lx)}{\cosh\left(l\ell_c/2\right)}\right), \tag{6}$$

where

$$l = \sqrt{G_v'(1+ih_v)\frac{pd_v^3}{4t_v}\frac{G_w J_w + G_c J_c}{G_w J_w G_c J_c}}. \tag{7}$$

Integrating (6) again we find the inner and outer tube twist angles $q_c(x)$ and $q_w(x)$, the torsional shear strains and stresses in the inside and outside tubes, the shear strain through the thickness of the visco-elastic layer, and the average torsional stiffness $k_t$ (a complex number):

$$k_t = \frac{G_w J_w + G_c J_c}{1 + \dfrac{2}{l\ell_c}\dfrac{G_c J_c}{G_w J_w}\tanh\left(l\ell_c/2\right)}. \tag{8}$$

From Eq. (8), the axial stiffness $k_{ax}$ and axial loss factor $h_{ax}$ of the coiled spring can be calculated using classical coil spring relations[7],

$$k_{ax} = \frac{4\Re e(k_t)}{npD^3}, \quad h_{ax} = \frac{\Im m(k_t)}{\Re e(k_t)}, \tag{9}$$

where the coil geometry is defined by the mean coil diameter $D$, and number of active turns $n$.

### 3.2 Validation

A 40mm straight length of 3 layer CLD torsion tube was analyzed with NASTRAN (Fig. 5). Both the inside and the outside tube are stainless steel in this example. The mid layer is a hypothetical visco-elastic material with a 50% loss factor. A single layer of quadratic solid elements (20 node bricks) is used to represent each layer of the assembly[8]. The outside tube is supported at one end and loaded with a distributed tangent load at the other; the resultant of the applied loads is an axial torque of 400 Nmm. Figure 5 compares the results from the NASTRAN analysis to those from the closed form analysis presented above. The twist angles of the inside and outside tube are shown as a function of $x$ in the top chart (both angles measured with respect to the mid section at $x$ = 0). The bottom chart shows the "through-the-thickness" shear strain in the visco-elastic layer. Excellent agreement is observed.

As expected, the shear in the visco-elastic layer is maximum at either ends of the inside tube section and corresponds to the local difference in twist angle between the inside and outside tube. The inside tube twists slightly in response to the torque transmitted through the visco-elastic layer. Maximum torsional shear stresses occur at $x$ = 0 in the inside tube and $x = \pm\ell_c/2$ in the outside tube.

For validation of the predicted damping ratio, a large inertia was attached to the periphery of the tip of the outside tube in place of the load. This creates a low frequency twisting mode in the torsion tube. A complex eigenvalue solution gives a loss factor for that mode equal to 4.62%. This compares favorably to the 4.68% predicted by equation (9).

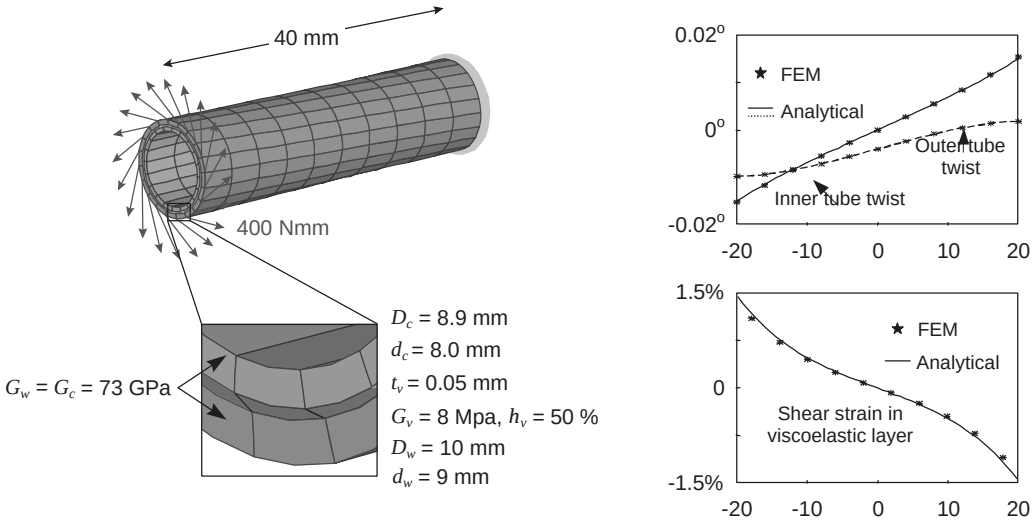


**Figure 5: Finite element (NASTRAN) solution for single section of torsion rod compared to closed-form analytical solution.**

## 4. MANUFACTURING ISSUES AND MATERIAL SELECTIONS

Material selections for this spring design are intimately related to the manufacturing process. Inner tube sections are cut to length then threaded and spaced on a stretched rubber core (that core is used only for manufacturing reasons and is not expected to contribute significantly to the damping); releasing the stretch produces an interference fit between the core and the constraining tube sections, holding these in place. One end of the soft visco-elastic layer is then attached around one end of this core. The whole assembly is then generously covered with epoxy adhesive and pulled into a slightly oversized outer tube. Before the epoxy has time to set, the tube is swaged to produce a tight fit around the damping layer and core and eliminate excess glue, then coiled on a mandrel. The assembly is then cured at room temperature and the ends are trimmed and machined to receive the end caps which are electron-beam welded in place. Finally, the finished coils are thoroughly cleaned to ultra-high vacuum standards.

### 4.1 Constraining layer sections

During coiling, there is tendency for the edges of the inner tube sections to dig into the soft visco-elastic layer. To mitigate this problem, a pliable (low yield point) but stiff (high modulus) material must be used for these inner tube sections. A 6061-O, annealed aluminum alloy was selected. The edges of the tube sections are also rounded to minimize pressure into the damping layer.

### 4.2 Visco-elastic material

To maximize damping, the visco-elastic layer must be as thin as possible. However, extremely thin layers are difficult to handle and would require tight tolerances on the diameters of the tubes and the swaging operation. A thickness of the order of .010" (0.25mm) is considered a minimum. A relatively stiff visco-elastic material is required so that there is significant elastic energy in the damping layer (see Section 5.1). DYAD 606, manufactured by Soundcoat[9], was selected. It is available in .020" (0.51mm) thickness, has very high loss factor (105% at 10 Hz) and relatively large shear modulus, and is pliable enough for wrapping around the inner tube sections. This material is not self adhesive. A flexible epoxy glue must be used bond it to the metal surfaces.

### 4.3 Outer tube material

Large plastic strains are induced in the outside tube during coiling (hot forming is excluded because of the presence of the visco-elastic materials inside). Whatever material is used must be pliable enough to avoid cracking. Since the outside tube is also the load bearing component for the static load, a compromise must be found between high yield and formability. Phosphorous bronze was selected. It is traditionally used for various cold formed elastic components and is available in various mill tempers obtained by cold work. For best spring properties (highest yield) the hardest possible temper must be used. However, harder tempers have lower ultimate strains and are more likely to crack during coiling. Coiling tests have led to the selection of a ¾ hard temper.

## 5. TREND STUDIES AND DESIGN OPTIMIZATION

### 5.1 Trend study

Looking at the relations in the Section 3.1, it is apparent that optimal proportions must exist for the diameters and thicknesses of the 3 layers, as well as the geometry of the coil that maximize net damping. A simple trend study gives an idea of the effects of the various design parameters as shown in Fig. 6. Note that $h_{ax}$ is frequency dependent; the loss factors in the figure are calculated at a fixed frequency (10 Hz in this example).

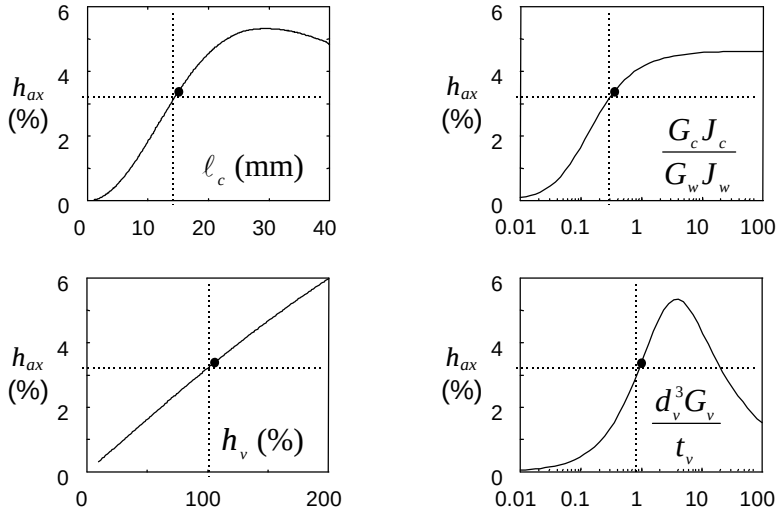


**Figure 6: Effects of various cross section parameters on net torsional damping.**

The 4 curves in the figure show the individual effects of 4 parameters on the loss factor: the length of the inner tube sections $\ell_c$, the torsional stiffness balance between the inner and outer tubes $G_c J_c / G_w J_w$, the loss factor of the visco-elastic layer $h_v$, and the stiffness measure of the visco-elastic layer $D_v^3 G_v / t_v$. These parameters were varied one at a time around a nominal configuration of aluminum, DYAD 606, and phosphor bronze, with $D_w$ = 6 mm, $t_w$ = 0.5 mm, $t_v$ = 0.25 mm, and solid inner sections of aluminum rod, with $\ell_c$ = 15 mm.

The following observations can be made:

- damping is very sensitive to $\ell_c$: when $\ell_c$ is large, loads transferred to the inner sections accumulate along their length and force them to twist, reducing the twist angle differential and the damping. If the sections are short, the twist angle differential at their ends is small and damping is again small. An optimal length (about 30 mm in this example) exists that maximizes damping. Note that this optimal length also depends on the values of the other 3 parameters.
- the torsional stiffness of the core must be large enough to minimize twist in the inner sections. The figure shows that for $G_c J_c / G_w J_w$ greater than about 1, the effect of this parameter is small.
- an increase in the loss factor of the visco-elastic layer leads to an almost proportional increase in net spring loss factor.
- the effect of the visco-elastic layer "stiffness" $d_v^3 G_v / t_v$ also shows the existence of an optimal value. This is explained by a balance condition between a stiff layer that induces large twist in the inner section, reducing shear strains and damping, and a soft layer which minimizes twist in the inner sections but also reduces the strain energy in the visco-elastic layer (because of its low modulus and/or large thickness).

### 5.2 Design Optimization

Since many different variables have strong and coupled effects on the final performance and the trend study shows the existence of optimal values, we used numerical optimization techniques to lead us to favorable proportions for the cross section and coil. The objective is to maximize characteristic deflection $d_{\max}$ of the spring while providing at least 3% axial loss factor and satisfying a number of additional conditions. Note that the spring loss factor is a weak function of frequency; to formulate the optimization problem, a fixed target frequency of 10 Hz was chosen. The static load capacity is defined as the compressive load to 80% solid length. Other design criteria (loads to yield, solid length, first surge natural frequency, etc.) are evaluated using classical methods for coil springs[7] which will not be detailed here.

Also note that the Q's of an actual isolation system built on these springs will in fact depend on both the axial and the transverse loss factors. However, transverse deformations of a coil spring are more complex and difficult to analyze than pure axial deformations, so they are not included in the formulation of the optimization problem. Transverse deformations involve a combination of torsion and bending in the spring "wire". Assuming for example an even distribution of the total elastic energy between bending and torsion, and assuming that the bending deformations are undamped, the transverse loss factor of the spring could be expected to fall around ½ of the axial value (i.e. 1.5 %).

The optimization problem was formulated as follows:

**ADJUST**

cross section geometry : $d_c, t_c, t_v, t_w$

constraining section length : $\ell_c$

Coil Geometry : active length $L$, pitch $p$, mean coil diameter $D$

**TO MAXIMIZE**

characteristic deflection $d_{\max}(10\text{ Hz})$

**SUCH THAT**

net loss factor $h$ (10 Hz) > 3%

Number of section per turn $pD/\ell_c > 6$

Spring index $c = D/D_w > 5$

pitch angle $a < 12°$

active turns $n = L/p > 2$

viscoelastic layer diameter to thickness ratio $d_v/t_v > 10$

first resonant frequency $f_1 > 400$ Hz

active length to coil diameter ratio (buckling) $L/D < 2.5$

Static load capacity 445 N (100 lbs) < $P_{\max}$ < 1334 N (300 lbs)

max. active length $L < 50$ mm

load to yield > load to solid length

where the cross section is defined by the inside diameter of the inner tube sections $d_c$, and the thicknesses of the inner tube $t_c$, damping layer $t_v$, and outer tube $t_w$. The analysis was coded in MATLAB[10] and the optimization problem was solved using MATLAB's multivariable constrained minimization routine. The results of the optimization are summarized in Tables 1 and 2. The tables also list side constraints (limits on ranges for design parameter values) and final values of the constraints.

| | Parameter | Symbol | Units | limit | **Optimum value** | Upper Limit |
|---|---|---|---|---|---|---|
| 1 | constraining section ID | $d_c$ | mm | 0 | ***5*** ® | 5 |
| 2 | constraining section wall | $t_c$ | mm | 0.3 | ***0.93*** | 3 |
| 3 | damping layer thickness | $t_v$ | mm | 0.51 | ¬ ***0.51*** | 2 |
| 4 | outer tube wall | $t_w$ | mm | 0.5 | ***0.80*** | 3 |
| 5 | constraining layer length | $\ell_c$ | mm | 5 | ***29.08*** | 50 |
| 6 | coil free active length | $L$ | mm | 10 | ***31.07*** | 180 |
| 7 | coil pitch | $p$ | mm | 1 | ***13.37*** | 60 |
| 8 | coil mean diameter | $D$ | mm | 10 | ***55.55*** | 100 |

**Table 1: Design parameter values for final design from MATLAB optimization run; active side constraints are identified with arrows.**

| | Constraint Description | Symbol | Units | Limit | Constraint value at optimum |
|---|---|---|---|---|---|
| 1 | minimum loss factor | $h$ | % | > 3 | ¬ ***3*** |
| 2 | minimum # constraining layer sections per turn | $pD/\ell_c$ | - | > 6 | ¬ ***6*** |
| 3 | minimum spring index | $D/D_w$ | - | > 5 | ***5.86*** |
| 4 | maximum pitch angle | $a$ | deg | < 12 | ***4.4*** |
| 5 | minimum # active turns | $L/p$ | - | > 2 | ***2.3*** |
| 6 | minimum diameter/thickness, damping layer | $d_v / t_v$ | - | > 10 | ***14.5*** |
| 7 | minimum coil surge frequency | $f_1$ | Hz | > 400 | ¬ ***400*** |
| 8 | maximum L/D for coil stability (column buckling) | $L/D$ | - | < 2.5 | ***0.56*** |
| 9 | minimum static compressive load capacity | $P_{max}$ | N | > 445 | ¬ ***445*** |
| 10 | maximum static load compressive capacity | $P_{max}$ | N | < 1334 | ***445*** |
| 11 | maximum active length (space available) | $L$ | mm | < 50 | ***31.1*** |
| 12 | safety against yield at solid length | $P_{max}/P_{solid}$ | - | > 1 | ¬ ***1*** |

**Table 2: Constraint values for final design from MATLAB optimization run; active constraints are identified with arrows.**

## 6. FINAL DESIGN

Availability of materials and manufacturing constraints led to a final design (as manufactured, Fig. 7) slightly different from the optimal design of Table 1. To the approximately 2.5 active turns called for by the optimizer, end coils (3/4 turn at each end) are added to provide interface with the stack elements. Because of the tubular cross-section and the small axial clearance between coils, achieving flat end coils normal to the spring axis is not possible. Instead, seats are used to provide support at each end of the spring. Rigid plastic seats (molded epoxy) were used for the prototypes and initial tests. Note however that in the LIGO isolation stacks, the springs will be mounted on softer, molded Fluorel[2] rubber seats. These softer seats attenuate transmission of acoustic disturbances through the stack. They also provide additional damping, principally in the shear direction.

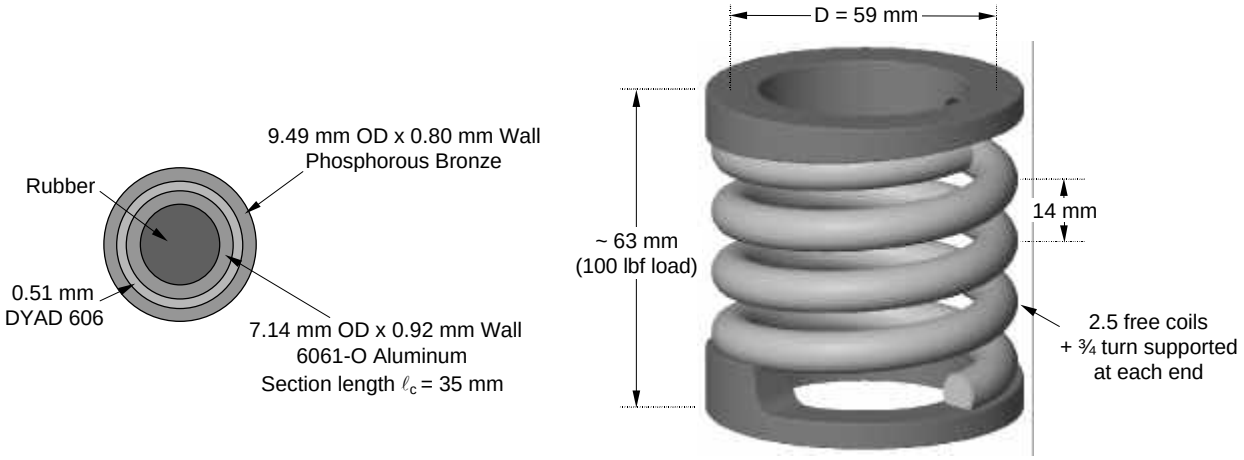


**Figure 7: Final design of the CLD coil spring; the spring is sitting seats for interfacing with flat mass elements.**

## 7. PROTOTYPING AND TESTING

As part of the development efforts for this design, several prototype springs were produced and subjected to a variety of static and dynamic tests. Results from those tests were in general very consistent from one prototype to another. One of those prototypes and some of the tests that were performed on it are described in the following subsections.

### 7.1. Coil Spring Prototype

The left-hand side of Fig. 8 shows a coil spring prototype with the molded epoxy seats that were used for the tests. In the right hand side of the figure, a photograph of a cross section through an actual spring shows the internal structure.

Note the slight “crushing” of the damping layer near the ends of the constraining sections; the internal geometry is otherwise very regular and undisturbed by the severe coiling deformations.

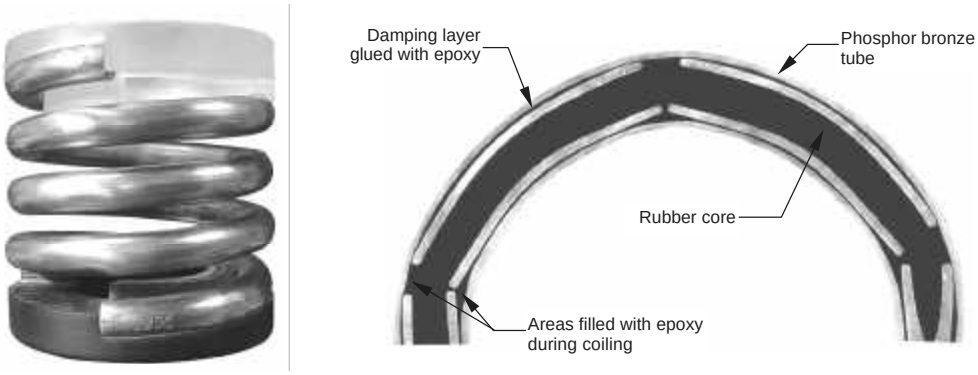


**Figure 8: Coil spring prototype ready to be tested and cross section through an actual spring showing internal structure.**

### 7.2. Static Testing

The prototype was first tested for static load capacity and yield in a load frame. It was first subjected to 5 cycles of compressive loading to nominal deflection (80% of deflection to solid length) to detect any yield, then 1000 cycles of compressive loading to 95% of solid length to detect any fatigue problems. The results of the 5 cycles are plotted in Fig. 9. They show no evidence of yielding and confirm a load capacity of about 445 N (100 lbf) at 80% solid length. The fatigue tests showed no evidence of degradation of the outer tube or internal structure.

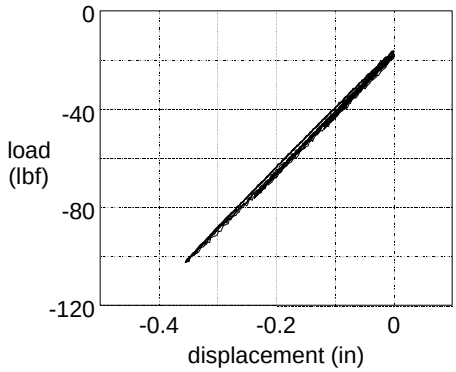


**Figure 9: Static testing of prototype coil spring (5 cycles from 0 to approximately 80% of deflection to solid length).**

### 7.3. Dynamic Testing

A special instrument was designed and constructed to allow measuring the dynamic stiffnesses and loss factors of the springs at low frequencies. The apparatus uses the rotational inertia of a large, symmetric, horizontal pendulum to produce low frequency resonance of the single degree of freedom system formed by the pendulum and the spring being tested. Variable amounts of mass can be attached at the tips of the beam to vary the inertia of the pendulum and the frequency of the measurement without affecting the static preload on the spring. Instrumentation measures the free decay of the pendulum oscillation and post-processing provides loss factors and stiffnesses of the springs.

The setup is shown in Fig. 10. The pendulum beam is a 1.3 m long steel box beam, with plates welded at the ends to support extra tip masses. It is supported at its center on a brass flexure. Two stops limit the swing of the pendulum to protect the flexure. The whole system is built on a massive steel and concrete base. A non-contact inductive displacement probe is mounted on the base on one side of the flexure. The spring can be mounted at one of two locations, depending on whether axial or shear properties will be measured. Each location features an adjustable "U" bracket attached to the pendulum beam. That bracket allows for adjustment of the spring static preload. When the spring is mounted in the axial location, a counterweight (Fig. 10, left) is bolted on top of the pendulum beam to provide the nominal axial preload on the spring (100

lbf), and the "U" bracket is used to adjust the pendulum initial position. When the spring is mounted in the shear position, the counterweight is removed, the "U" bracket adjusts the preload, and the flexure resists the resulting twisting moment.

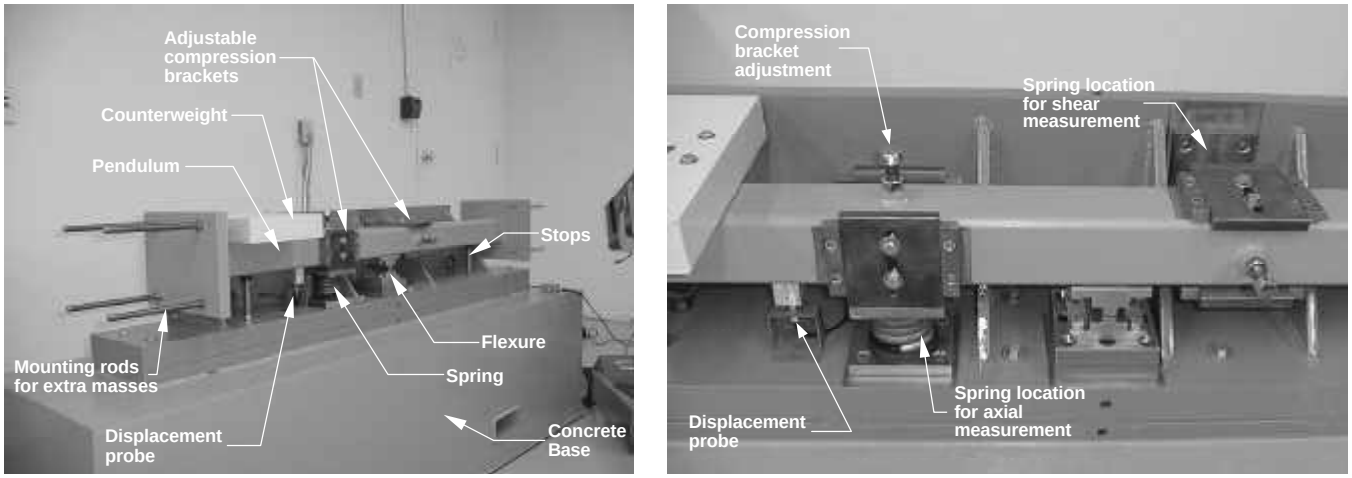


**Figure 10: Low frequency spring testing apparatus.**

Measurements are taken by exciting the pendulum by hand and recording probe signal versus time during free decay. The data is acquired such that the initial peak to peak spring deflection amplitude is consistently equal to about 65 μm in the axial setup and 48 μm in the shear setup (tests have shown that at those amplitudes, there is no amplitude dependence in the measured stiffness and damping). A least square fit to that data, together with calculated mass properties of the setup, provides a measure of the total rotational stiffness around the hinge line and total damping in the system. Corrections are applied to account for other sources of stiffness in the system: the bending stiffness of the flexure (less than 4% of spring effect), and a negative stiffness effect due to gravity and the position of the pendulum center of mass above the hinge line (less than 3% of spring effect).

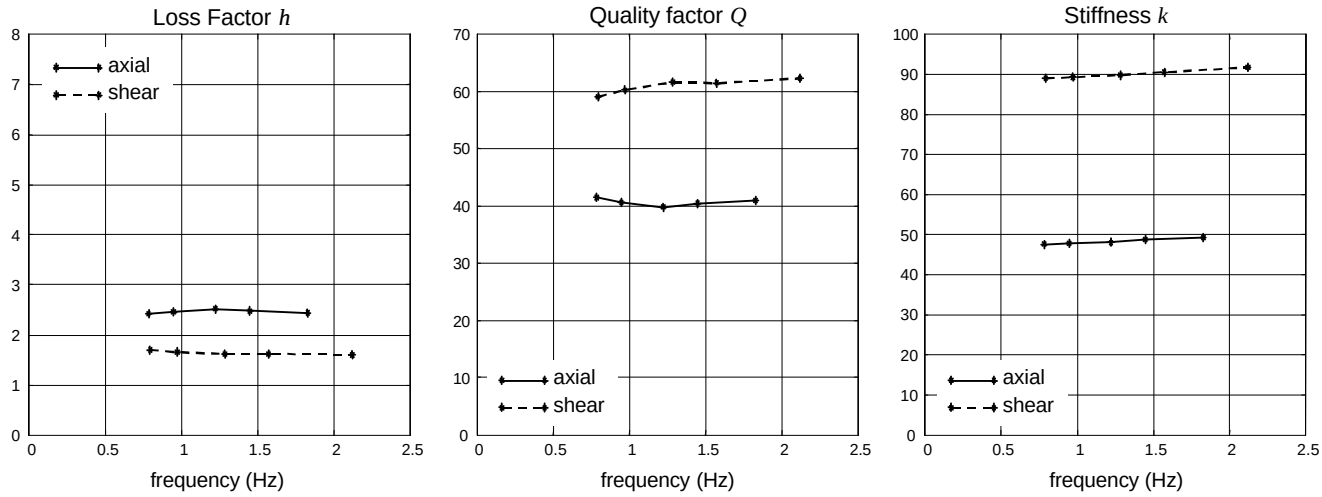


**Figure 11: Loss factor, quality factor, and stiffness in axial and shear directions of coil spring prototype on epoxy seats as a function of frequency. Temperature during tests was between 21.0 and 21.5 ºC.**

Figure 11 shows the dynamic test results obtained on a prototype coil on molded epoxy seats. The figure shows axial and shear loss factors, quality factors, and dynamic stiffnesses as a function of the frequency of the free decay oscillation. Note how the apparatus described above allows for frequency adjustments from about 0.8 to about 2.2 Hz by changing the amount of mass mounted at the pendulum tips. As expected, the results show weak frequency dependence. The axial loss factor is about 2.5% or 16% lower than expected. The transverse loss factor is around 1.6%, or 64% of the axial value. Note that the 3% value obtained in the optimization was calculated at 10 Hz; other dynamic tests, not described here, have shown axial loss factors in the 2.4 to 2.8% range between 5 and 10 Hz. The corresponding quality factors are between

40 and 62, well below our LIGO requirement of 70. Note also that the spring is about 2 times stiffer in the transverse direction as in the axial one.

Models of the LIGO isolation stacks build with these springs predict performance measures that satisfy the requirements. Note also that the actual stacks will make use of molded Fluorel[2] seats in place of the stiff epoxy seats used in the tests reported above. There are two primary reasons for this: first, with stiff seats there is a concern of stick-slip noise appearing at the interface between the coil and the seat, and second, the softer rubber seats attenuate transmission of acoustic disturbances through the spring (acoustic performance has been demonstrated through testing). Another effect of the Fluorel[2] seats is a substantial increase in the tranverse loss factor: measured loss factors on rubber seats are around 6% ($Q \sim 17$). The axial loss factor is also slightly increased to about 3.2%.

## 8. CONCLUDING REMARKS

A new application of constrained layer damping to torsional deformations has been developed and used to design an internally damped coil spring. The spring is entirely sealed inside a metal envelope, which makes it appropriate for vibration isolation applications inside ultra-high vacuum systems. Explicit analytical expressions were derived for approximate evaluation of the frequency dependent stiffness and damping of the spring. Those expressions were used for trend studies followed by formal optimization of the design, maximizing isolation (i.e. softness) with an upper limit on the quality factor ($Q$) to limit resonant oscillations of the isolation system. The optimization resulted in a practical design with an expected $Q$ of 33 at 10 Hz. Manufacturing processes were developed and prototype springs were produced that were thoroughly tested and exhibited mechanical properties very close to expectations. The spring can support 445 N (100 lbf) of axial compressive load, with an axial deflection of about 8.5 mm, and a measured axial $Q$ of about 40 at 1 to 2 Hz. With that spring, isolation stacks have been designed that satisfy the very strict seismic isolation requirements for the LIGO detectors. As of January 1998, about 10 prototypes have been produced and tested, and another 4000 springs are planned for fabrication by the end of the year.

## 9. ACKNOWLEDGEMENTS

This work was funded by the National Science Foundation, under contract #PC185630 between Hytec, Inc. and the California Institute of Technology. Patents for the design described in this paper as well as a number of variants based on the same concept are pending (SN 08/972,030, November 17, 1997). The government has certain rights to the invention. The authors wish to thank Steve Sowa and others at Pegasus Manufacturing, Inc., in Hamden, CT, for rising up to the challenge of manufacturing this device and for their input regarding manufacturing processes.

## 10. REFERENCES

1. The LIGO Project, Project Office at Caltech (818) 395-2129, http://www.ligo.caltech.edu.
2. Fluorel®, registered trademark of 3M/Dyneon, 3M Center, Bldg 220-10E-10, St Paul, MN 55144-1000, (800) 635-8061.
3. Shiau, Jgi J., "Inherently Effectively Damped Doiled Spring," U.S. Patent #4640500, Feb. 3, 1987.
4. Sandt, Hartley, "Composite Structural Element and Process for Making Same," U.S. Patent #5576081, Nov. 19, 1996.
5. Jones, David I. G., "Application of Damping Treatments," Chapter 37 in *Shock and Vibration Handbook*, 3rd Ed., Cyril M. Harris, Editor, McGraw-Hill, 1987, pp. 37-1 to 37-34.
6. Plunkett, R. and Lee, C. T., "Length Optimization for Constrained Layer Damping," *Journal of the Acoustical Society of America*, Vol. **48,** No. **1,** Pt. 2, pp. 150-161, 1970.
7. Wahl, A. M., *Mechanical Springs*, 2nd Ed., McGraw-Hill, 1963.
8. Johnson, C. D. and Kienholz, D. A., "Finite Element Prediction of Damping in Structures with Constrained Layer Viscoelastic Layers," *AIAA Journal*, pp. 1284-1290, September 1982.
9. Soundcoat® Bulletin 701, "DYAD for use in Thick Plate Vibration Damping" and Bulletin 810, "Constrained Layer Damping Materials for Control of Noise and Vibration," Soundcoat, 1 Burt Dr., Deer Park, NY 11729.
10. MATLAB Users' Manuals, The Mathworks, Inc., 24 Prime Park Way, Natick, MA 01760, http://www.mathworks.com.